www.cadanda.com
Computer-Aided Design AND APPLICATIONS

A Novel Approach to Metallographic Grain Size Measurement Using Deep Learning and Computational Geometry Techniques

Xiang Li[1], Yiming Yuan[2], Ling Chen[3], Shuai Guan[4], Shuai Feng[5], Sara McMains[6]

[1]Research Institute of Advanced Materials, CISRI Group, xli@berkeley.edu
[2]Research Institute of Advanced Materials, CISRI Group, yym11267@163.com
[3]China Railway Siyuan Survey and Design Group, hust_chenling@outlook.com
[4]Research Institute of Advanced Materials, CISRI Group, shuai.guan@connect.polyu.hk
[5]Research Institute of Advanced Materials, CISRI Group, shuaifeng365@outlook.com
[6]UC Berkeley, mcmains@berkeley.edu

Corresponding author: Xiang Li, xli@berkeley.edu

Abstract. Grain size measurement from high-resolution metallographic microscope images is a fundamental task in materials science, as microstructural grain characteristics critically determine material properties. Traditional manual methods are labor-intensive and prone to human bias, while existing automatic approaches often suffer from segmentation noise, artifacts, and incomplete boundaries, limiting their effectiveness in large-scale screening applications. To overcome these limitations, we propose a novel, automated framework that integrates deep learning and computational geometry techniques for accurate and efficient grain size measurement. Our approach employs a U-Net model for initial grain boundary segmentation, followed by a specially designed skeleton-based cleaning process that removes noise and spurious branches while preserving genuine boundaries. This refined boundary representation enables precise grain size computation using the intercept method in accordance with ASTM E112 standards. Experimental evaluations on diverse, real-world metallographic datasets demonstrate that our method achieves a mean absolute error of 0.034 in grain size measurement and reduces processing time from 99 seconds (manual) to approximately 5 seconds per image. These results underscore the potential of our integrated approach as a robust and scalable solution for advancing metallographic analysis in both research and industrial applications.

Keywords: metallography, grain size measurement, topological skeleton, materials characterization
DOI: https://doi.org/10.14733/cadaps.2026.451-461

1 INTRODUCTION

Metallography is the analysis of microscopic images of materials to characterize their internal features, such as grains, phases, and inclusions. It is essential in materials science because these microstructural characteristics strongly influence properties such as strength, toughness, and corrosion resistance. Accurate metallographic analysis plays a critical role in optimizing the performance and reliability of metal materials, especially in safety-critical and high-performance applications across industries such as automotive manufacturing, aerospace, small arms safety, and structural engineering. Among various metallographic assessments, grain size measurement is particularly important, since the average grain size often governs key performance attributes of the material [6, 21]. Despite its significance, grain size measurement remains predominantly manual [1], making it time-consuming and susceptible to human bias.

Automated image processing methods have become an essential tool in microstructure analysis within materials science [3, 14, 15]. These techniques enable the quantitative characterization of features such as grain boundaries, phases, and inclusions by employing standard methods such as thresholding, morphological filtering, and watershed segmentation. Such approaches reduce the reliance on manual analysis while providing detailed microstructural information.

In the context of grain size measurement, these techniques have proven particularly effective. For example, Peregrina-Barreto et al. applied a combination of image enhancement and segmentation techniques to automatically delineate grains and boundaries, noting that factors such as noise and low contrast can compromise image quality and segmentation accuracy [18]. Similarly, Paredes-Orta et al. developed a watershed-plus-marker method based on an improved ultimate opening function, which accurately detects grain markers even in poor quality images [17]. Banerjee et al. introduced a sequential processing pipeline that extracts closed grain contours from optical micrographs, yielding grain size distributions comparable to those obtained via conventional methods [2]. In addition, Flipon et al. demonstrated that image analysis of both optical and scanning electron micrographs can accurately determine grain size distributions while significantly reducing processing times compared to traditional electron backscattered diffraction techniques [7]. Furthermore, Li et al. proposed an algorithm that automates the intercept method for grain size measurement by applying a topological skeleton approach to extract continuous and closed grain boundaries, thereby accurately determining the average grain size in accordance with international standards [13]. Although these rule-based algorithms perform well when grain boundaries are sharply defined, they frequently encounter difficulties when applied to complex microstructures or images with variable quality, thereby limiting their generalizability across different materials and imaging conditions [12, 13].

Machine learning and deep learning techniques have emerged as powerful tools in microstructure analysis, enabling robust and adaptable grain size measurement across diverse material types and imaging conditions. These data-driven approaches excel when high-quality training data is available, as they can learn complex features and generalize well to varying imaging scenarios. However, their performance can be affected by suboptimal training data or tuning parameters.

In particular, Gajalakshmi et al. developed an algorithm based on support vector regression that utilizes features extracted from edge-detected images to count grains and accurately determine grain size [8]. Similarly, Li et al. implemented a multi-task learning framework combined with a generative adversarial network to concurrently detect grain boundaries and segment second phase particles, achieving high accuracy in both tasks [11]. Choudhary et al. integrated traditional machine learning with deep learning models to classify microstructural regions in sintered NdFeB magnets from Kerr microscopy images, with results compared against electron backscatter diffraction data [5]. Furthermore, Gorynski et al. introduced a region-based convolutional neural network approach to quantify microstructural characteristics, yielding consistent and statistically precise grain size measurements [9]. While these approaches are highly adaptable, they may introduce recognition errors or overlook certain boundaries when the training data or tuning parameters are suboptimal, and they may also encounter challenges related to insufficient data [19].

To address these shortcomings, we propose a novel approach that combines deep learning-based segmentation with specially designed post-processing steps using computational geometry concepts. In particular, our method incorporates advanced topological skeleton analysis to enhance the overall quality of the grain boundary representations. This integration improves the continuity and clarity of the boundaries by mitigating noise and discontinuities typically associated with the segmentation process. Validated on real-world metallographic datasets, our approach is efficient, scalable, and demonstrates robust performance across diverse microstructures and preparation conditions. This performance bridges traditional metallography with computer-aided design (CAD) techniques, enabling automatic and reliable grain size measurement, and advancing metallographic analysis.

2 MATERIALS

In this research, a total of 400 metallographic images were acquired for model training and validation. Among these, 300 images exhibit sharply defined grain boundaries and were prepared under optimal conditions, including cutting, grinding, polishing, and etching, to ensure clarity of microstructural features. These 300 images are evenly divided between high-purity iron (150 images) and stainless steel (150 images), providing a balanced representation of materials with distinct microstructural characteristics. Additionally, 100 images of high-purity iron prepared under assorted conditions were incorporated to enhance the generalization ability of our algorithm and mitigate overfitting to ideal imaging scenarios. This diverse dataset enables our integrated algorithm to learn robust microstructural features across varying preparation conditions and material types, thereby reinforcing the accuracy and generalizability of both the deep learning segmentation and the computational geometry-based post-processing stages.

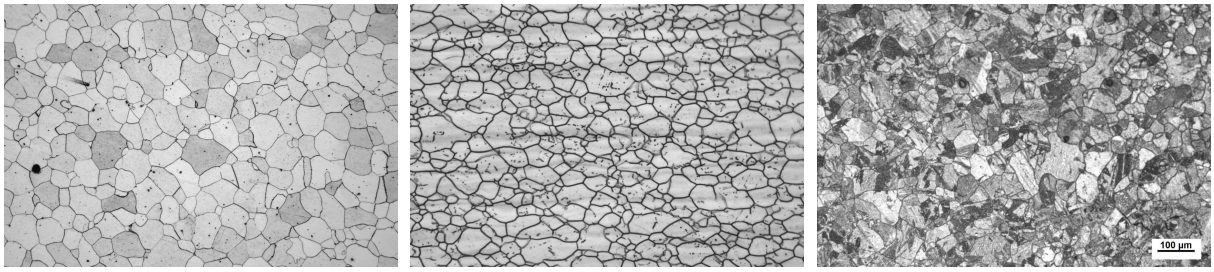

Figure 1: Representative metallographic images of three specimen categories: (a) high-purity iron prepared under optimal conditions, (b) stainless steel prepared under optimal conditions, and (c) high-purity iron prepared under assorted conditions. Images obtained under optimal conditions exhibit sharply defined grain boundaries compared to those prepared under assorted conditions.

Figure 1 illustrates representative examples of the three categories of metallographic images used in this study, highlighting the visual differences between specimens prepared under optimal and assorted conditions. Table 1 summarizes the key details of the specimen materials and the associated metallographic preparation protocols, including the procedures for cutting, grinding, polishing, etching, and microscopy. Together, these representations provide essential context for our experimental framework and support the comprehensive evaluation of our algorithm's performance across a broad spectrum of microstructural features.

	High-purity Iron (Optimal)	Stainless Steel (Optimal)	High-purity Iron (Assorted)
Image Count	150	150	100
Microstructure	Ferrite (grain)	Austenite (grain)	Ferrite (grain)
Cutting	Metallographic cutting machine		Assorted
Grinding	1000-grit sandpaper		Assorted
Polishing	Polishing cloth		Assorted
Etching	Nital	1g $KMnO_4$ +10ml H_2SO_4 +90ml H_2O	Assorted
Microscopy	Leica DMi8C microscope Magnification: 100x or 200x Image size: 5472 × 3648 pixels		

Table 1: Summary of specimen materials and corresponding metallographic preparation protocols

3 ALGORITHM DETAILS

Our proposed approach for automatic grain size measurement comprises three key stages: grain boundary extraction, grain boundary cleaning, and grain size computation using the intercept method. Figure 2 illustrates the overall structure of our approach and provides representative examples of the intermediate results obtained at each stage.

1. **Grain Boundary Extraction:** In the initial stage, we train and deploy a U-Net model to segment grain areas and grain boundary regions from input metallographic images. While U-Net effectively identifies the majority of grain boundaries, it may also detect some grain boundary artifacts and feature imperfections due to segmentation inaccuracies and the inherent complexities of material structures.

2. **Grain Boundary Cleaning:** The second stage involves refining the extracted grain boundaries through a topological skeleton-based cleaning process. Utilizing computational geometry concepts, we analyze the main boundary topologies and iteratively remove minor, dangling branches while retaining larger or more complete branches that correspond to genuine grain boundaries. This process minimizes the impact of artifacts and imperfections, ensuring a more accurate representation of the grain structure.

3. **Grain Size Computation:** Finally, we apply the intercept method, a standardized technique for grain size measurement, to quantify grain sizes based on the cleaned grain boundaries. The intercept method involves overlaying test patterns on the metallographic images and calculating grain size by counting the intersections of these patterns with the grain boundaries. Our approach mitigates the intercept method's sensitivity to small noisy areas and its insensitivity to broken grain boundary ends by integrating the previous stages, thereby enhancing the overall accuracy and reliability of grain size measurements.

Figure 3 presents a flowchart summarizing our proposed algorithm. Further details on the implementation of each stage are provided in the remainder of this section.

3.1 Grain Boundary Extraction

We utilize the U-Net architecture [20] to segment grain boundaries from metallographic images. U-Net is a well-established model for semantic segmentation and is suitable for high-resolution microscopy data, enabling a clear distinction between grain boundary regions and grain areas.

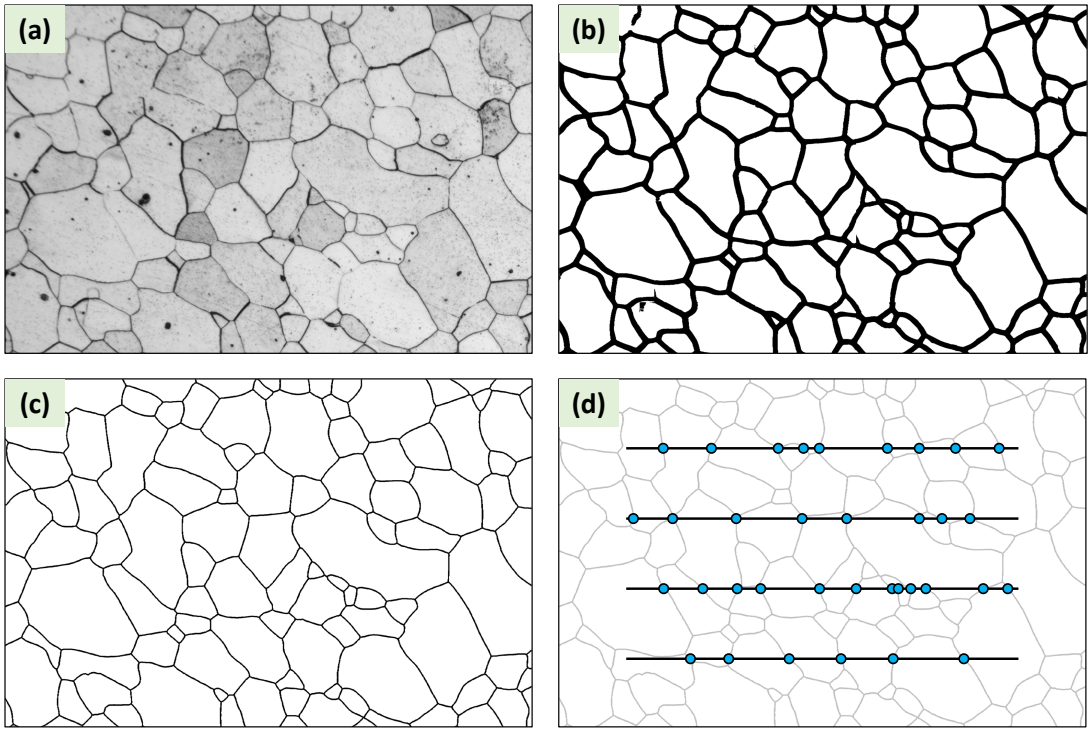

Figure 2: Overview of the proposed approach for automatic grain size measurement. The representative image example shows the key stages involved: (a) input metallographic image, (b) grain boundary extraction using the U-Net model, (c) grain boundary cleaning using a topological skeleton-based process, and (d) final grain size calculation via the intercept method

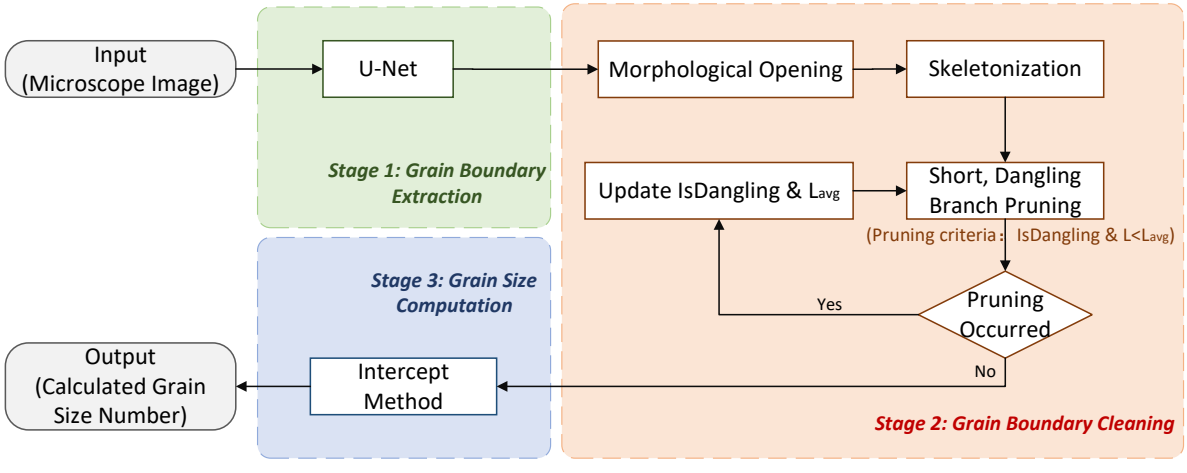

Figure 3: Flowchart summarizing our proposed algorithm

A dataset of 400 real-world metallographic images was collected and labeled (as discussed in Section 2), encompassing materials such as high-purity iron and stainless steels produced and imaged under diverse conditions. Each image was systematically partitioned into 512×512 patches with a stride of 128, a process that both expands the dataset and mitigates computational demands during training. These patches were then split into training (60%), validation (20%), and testing (20%) sets. Additionally, the same testing subset was manually annotated for grain size measurement using the intercept method, thus enabling an overall evaluation of our complete approach.

Traditional U-Net, as originally proposed, requires input images of size 572×572 and produces outputs of size 388×388 [20], which necessitates cropping during the skip connections to align the feature maps. This discrepancy arises from the use of the *valid* padding strategy in convolution operations, where the output size decreases by two pixels after each convolution. In contrast, the *same* padding strategy preserves the input dimensions by zero-padding the image borders appropriately. In our implementation, we adjust both the input and output sizes to 512×512, thereby eliminating the need for cropping and preserving spatial resolution throughout the network. This modification facilitates direct concatenation in the skip connections and enhances the effective use of multi-scale features for precise grain boundary segmentation. The U-Net architecture used in our implementation is depicted in Figure 4.

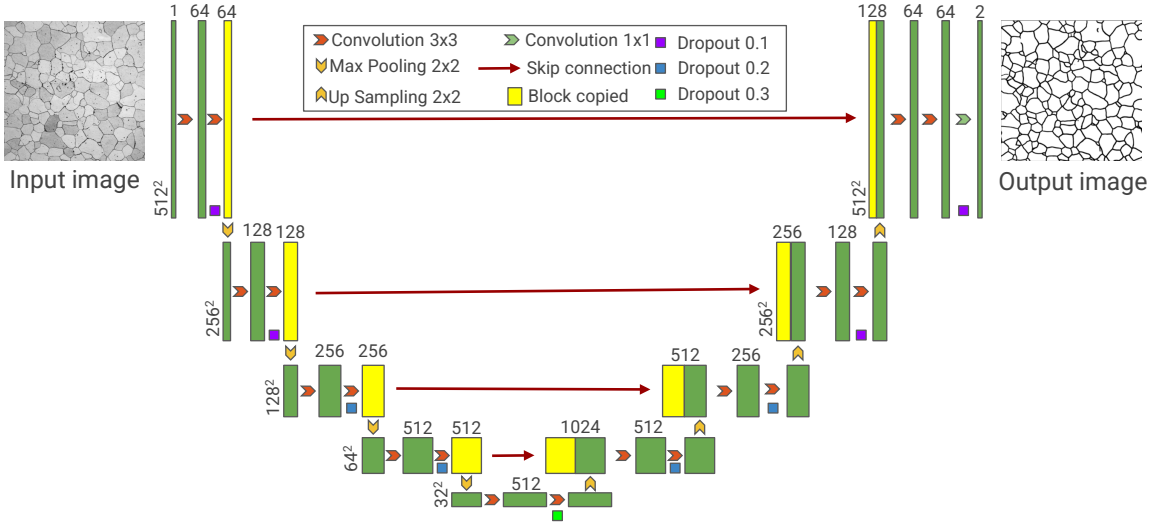

Figure 4: Our variant of the U-Net architecture for grain boundary extraction

To mitigate the risk of overfitting, several regularization strategies were integrated into our training process. Specifically, dropout layers with a rate of 0.3 were inserted after each convolutional block in the encoder path of the U-Net architecture, and L2 weight regularization with a coefficient of 1×10^{-4} was applied to the network parameters. Furthermore, data augmentation was performed using horizontal flipping, vertical flipping, 90° rotations in both clockwise and counterclockwise directions, and contrast enhancement. We also conducted 10-fold cross validation on the training set to ensure robust hyperparameter tuning and reliable performance evaluation.

Although U-Net successfully identifies the majority of grain boundaries, certain challenges remain. Noise introduced during metallographic preparation and incomplete etching can cause some impurities to be misclassified as boundaries, while partially corroded boundaries may be misclassified as grains. Consequently, actual boundaries may appear as dangling branches that are not fully connected, and other noise-like features may be erroneously labeled as valid boundaries. These artifacts can undermine the accuracy of subsequent grain

size measurements. Therefore, in the next step, we refine and correct the initially segmented boundaries to address these limitations.

3.2 Grain Boundary Cleaning

After the U-Net segmentation, we refine the identified grain boundaries by extracting their topological skeleton and removing incorrect segments. The skeleton representation simplifies the overall topology, enabling the differentiation of true grain boundaries from undesired artifacts such as segmentation noise and falsely detected structures within the microstructure.

In the topological skeleton, valid grain boundaries are represented by long, continuous edges. Both fully connected boundaries and discontinuous yet valid boundaries tend to manifest as longer branches that should be preserved, whereas short, dangling branches are more likely to represent noise or minor artifacts and are targeted for removal.

In our grain boundary cleaning process, we first employ a morphological opening operation to eliminate isolated noise and smooth the U-Net segmentation output. Following this, we construct the topological skeleton using the algorithm proposed by Lee et al. [10]. We then compute the average length of the skeleton edges and set a threshold at 50% of this average length to distinguish between long and short dangling branches. Branches shorter than this threshold are pruned from the skeleton. Since pruning may generate new short dangling branches, we iteratively update the skeleton, recalculate the average branch length, and repeat the pruning process until no additional short branches remain. This systematic and iterative approach ensures that the final skeleton accurately represents the true grain boundaries.

For a concise overview, the detailed flowchart for this stage is provided in Figure 3. Additionally, Algorithm 1 presents the pseudocode for the cleaning procedure.

Algorithm 1 Skeleton-Based Grain Boundary Cleaning

procedure SkeletonCleaning(I_{seg})
  $I_{\text{open}} \leftarrow$ MorphologicalOpening(I_{seg})
  $S \leftarrow$ Skeleton(I_{open})
  $L_{\text{avg}} \leftarrow$ AverageBranchLength(S)
  $T \leftarrow 0.5 \times L_{\text{avg}}$ ▷ Threshold set to 50% of average branch length
  pruningOccurred ← **true**
  while pruningOccurred **do**
    pruningOccurred ← **false**
    for each branch $b \in S$ **do**
      if IsDangling(b) **and** Length(b) $< T$ **then**
        $S \leftarrow$ RemoveBranch(S, b)
        pruningOccurred ← **true**
      end if
    end for
    if pruningOccurred **then**
      $L_{\text{avg}} \leftarrow$ AverageBranchLength(S)
      $T \leftarrow 0.5 \times L_{\text{avg}}$
    end if
  end while
  return S
end procedure

3.3 Grain Size Computation

Following grain boundary extraction and cleaning, the resulting skeleton captures continuous boundaries and retains any long, dangling branches that correspond to actual grain edges. This step is critical for the intercept method prescribed by ASTM E112 [1], which is relatively insensitive to small breaks in boundaries but highly sensitive to noise and artifacts. By removing short, spurious branches and preserving longer, valid edges, our approach ensures that subsequent grain size measurements accurately reflect the true microstructure.

The intercept method draws test patterns (e.g., lines or circles) over the metallographic image and counts the intersections between these patterns and the identified grain boundaries. From these counts, the official ASTM grain size number G is computed using the following formula [1]:

$$G = -3.288 \; - \; 6.643856 \times \log_{10}\Big(\frac{L}{M \times N}\Big), \tag{1}$$

where L is the total length of the test patterns in millimeters, M is the magnification factor of the microscope, and N is the number of intersections counted. By aligning with a widely recognized standard, this method enables our final grain size measurements to be directly compared across different laboratories and material systems.

4 RESULTS AND DISCUSSION

4.1 U-Net Segmentation

We evaluated the segmentation performance of our U-Net model on a test dataset of 80 real-world metallographic images (as discussed in Section 2 and 3.1) at a resolution of 5472×3648. For comparison, we also assessed two other well-known segmentation methods, namely Fully Convolutional Networks (FCN) [16] and DeepLab V3+ [4], using precision, recall, and Intersection over Union (IoU) as evaluation metrics. Table 2 summarizes the performance of these models on our dataset.

Model	Precision	Recall	IoU
FCN	87.5%	89.2%	78.9%
DeepLab V3+	89.8%	92.3%	82.5%
U-Net	**95.4%**	**92.5%**	**86.5%**

Table 2: Segmentation performance of FCN, DeepLab V3+, and U-Net on the test dataset

The results indicate that U-Net outperforms both FCN and DeepLab V3+ in terms of precision, recall, and IoU. U-Net's superior performance can be attributed to its encoder-decoder architecture with skip connections, which effectively combines high-level semantic information with low-level spatial details, an essential characteristic for accurately delineating the intricate grain boundaries in metallographic images.

Notably, U-Net exhibits slightly higher precision than recall, which indicates that its identified grain boundaries are highly reliable with few false positives, even though a small fraction of true boundaries may be missed. In grain size measurement, false positives, often arising from impurities or segmentation noise, can significantly distort the accuracy of the measurements. Therefore, minimizing false positives is crucial, and U-Net's performance in this regard is particularly beneficial. By ensuring that most detected boundaries are indeed genuine, U-Net provides a more robust foundation for subsequent grain size analysis.

Overall, these findings underscore the suitability of U-Net for our application, particularly in scenarios demanding high-fidelity segmentation of complex metallographic features.

4.2 Overall Performance

We invited three professional metallurgists, each with more than 20 years of experience in manual grain size measurement, to determine the grain size numbers for 80 test images using the intercept method with the same intercept test patterns employed by our algorithm. Ground truth was established only when all three experts reached unanimous agreement. Table 3 compares our integrated method (U-Net + Skeleton + Intercept) with other automatic approaches, including U-Net + Intercept and U-Net + Skeleton + Planimetric, as well as with manual measurements.

Approach	Mean Absolute Error	Implementation Time (s)
Manual (Ground Truth)	0	99.17
U-Net + Intercept	0.219	2.81
U-Net + Skeleton + Planimetric	0.148	4.90
U-Net + Skeleton + Intercept (Ours)	0.034	5.04

Table 3: Comparison of different grain size measurement approaches

The results indicate that our integrated method achieves the lowest mean absolute error (0.034 in ASTM grain size number) while processing each image in approximately 5 seconds, compared to roughly 99 seconds for manual measurement. Although the U-Net + Intercept approach is faster, its accuracy is significantly lower (mean absolute error of 0.219). These findings suggest that incorporating the skeleton-based cleaning process substantially improves segmentation quality, which in turn enhances the accuracy of grain size measurements. Overall, our approach not only reduces the time and effort required for manual analysis but also outperforms other automated methods in terms of both accuracy and robustness, making it well-suited for practical metallographic analysis.

4.3 Limitations and Future Work

Although our method demonstrates robust performance across a dataset of 400 metallographic images, it currently relies on training the deep learning model from scratch. In many materials science studies, acquiring a similarly large dataset can be cost-prohibitive and time-consuming, given the complex procedures involved in specimen preparation and imaging. Consequently, smaller research groups or specialized studies may find it challenging to compile sufficient high-quality images for effective model training.

A potential direction for future work would be to develop a pre-trained version of our U-Net model using the diverse dataset collected in this study. This model could then be fine-tuned with a relatively small set of new metallographic images from a different material system or microstructure, using transfer learning techniques to maintain high segmentation accuracy. Such an approach would substantially lower the barrier to entry for labs with limited data, allowing them to benefit from our boundary cleaning and grain size computation stages. Ultimately, this would make automated grain size measurement more broadly accessible while preserving the robustness and efficiency of our integrated method.

5 CONCLUSIONS

In this paper, we presented a novel approach for metallographic grain size measurement that integrates deep learning and computational geometry techniques. By employing the U-Net model for initial segmentation and a skeleton-based cleaning procedure to refine grain boundaries, our method effectively addresses common issues such as noise, incomplete etching, and branching artifacts. The subsequent application of the intercept

method, which follows the ASTM E112 standard, ensures that the final grain size measurements are both accurate and comparable across different laboratories.

Experimental evaluations on real-world metallographic datasets show that our approach achieves state-of-the-art accuracy among automatic grain size measurement methods, with a mean absolute error of 0.034 in grain size number. Additionally, it significantly improves efficiency by reducing the processing time to approximately 5 s per image, compared to 99 s for manual measurement. By retaining critical boundary information and eliminating noise, our integrated system provides a reliable, fast, and easily adaptable solution for a range of material systems and imaging conditions, making it a valuable tool for advancing metallographic analysis in both research and industrial settings.

ACKNOWLEDGEMENTS

The authors acknowledge the Powley Fund for supporting this work.

ORCID

Xiang Li, http://orcid.org/0000-0001-5936-8457
Yiming Yuan, http://orcid.org/0009-0008-2872-7320
Ling Chen, http://orcid.org/0009-0004-1086-8222
Shuai Guan, http://orcid.org/0000-0002-7300-4921
Shuai Feng, http://orcid.org/0009-0005-4545-0392
Sara McMains, http://orcid.org/0000-0002-7152-9409

REFERENCES

[1] ASTM E112-13(2021) Standard test methods for determining average grain size. Standard, ASTM International, 2021. https://www.astm.org/e0112-13r21.html.

[2] Banerjee, S.; Chakraborti, P.C.; Saha, S.K.: An automated methodology for grain segmentation and grain size measurement from optical micrographs. Measurement, 140, 142–150, 2019. http://doi.org/10.1016/j.measurement.2019.03.046.

[3] Campbell, A.; Murray, P.; Yakushina, E.; Marshall, S.; Ion, W.: New methods for automatic quantification of microstructural features using digital image processing. Materials & Design, 141, 395–406, 2018. http://doi.org/10.1016/j.matdes.2017.12.049.

[4] Chen, L.C.; Zhu, Y.; Papandreou, G.; Schroff, F.; Adam, H.: Encoder-decoder with atrous separable convolution for semantic image segmentation. In Proceedings of the European Conference on Computer Vision (ECCV), 801–818, 2018.

[5] Choudhary, A.K.; Jansche, A.; Grubesa, T.; Trier, F.; Goll, D.; Bernthaler, T.; Schneider, G.: Grain size analysis in permanent magnets from kerr microscopy images using machine learning techniques. Materials Characterization, 186, 111790, 2022. http://doi.org/10.1016/j.matchar.2022.111790.

[6] Figueiredo, R.B.; Kawasaki, M.; Langdon, T.G.: The role of grain size in achieving excellent properties in structural materials. Journal of Materials Research and Technology, 30, 3448–3462, 2024. http://doi.org/10.1016/j.jmrt.2024.04.059.

[7] Flipon, B.; Grand, V.; Murgas, B.; Gaillac, A.; Nicolaÿ, A.; Bozzolo, N.; Bernacki, M.: Grain size characterization in metallic alloys using different microscopy and post-processing techniques. Materials Characterization, 174, 110977, 2021. http://doi.org/10.1016/j.matchar.2021.110977.

[8] Gajalakshmi, K.; Palanivel, S.; Nalini, N.; Saravanan, S.; Raghukandan, K.: Grain size measurement in optical microstructure using support vector regression. Optik, 138, 320–327, 2017. http://doi.org/10.1016/j.ijleo.2017.03.052.

[9] Gorynski, C.; Frei, M.; Kruis, F.E.; Winterer, M.: Machine learning based quantitative characterization of microstructures. Acta Materialia, 256, 119106, 2023. http://doi.org/10.1016/j.actamat.2023.119106.

[10] Lee, T.C.; Kashyap, R.L.; Chu, C.N.: Building skeleton models via 3-D medial surface axis thinning algorithms. CVGIP: Graphical Models and Image Processing, 56(6), 462–478, 1994. http://doi.org/10.1006/cgip.1994.1042.

[11] Li, M.; Chen, D.; Liu, S.; Liu, F.: Grain boundary detection and second phase segmentation based on multi-task learning and generative adversarial network. Measurement, 162, 107857, 2020. http://doi.org/10.1016/j.measurement.2020.107857.

[12] Li, X.: Scalable geometric processing techniques with applications in characterizing additively manufactured composites. Doctoral dissertation, University of California, Berkeley, 2021.

[13] Li, X.; Cui, L.; Li, J.; Chen, Y.; Han, W.; Shonkwiler, S.; McMains, S.: Automation of intercept method for grain size measurement: A topological skeleton approach. Materials & Design, 224, 111358, 2022. http://doi.org/10.1016/j.matdes.2022.111358.

[14] Li, X.; Cui, L.; Shonkwiler, S.; McMains, S.: Automatic characterization of spherical metal powders by microscope image analysis: a parallel computing approach. Journal of Iron and Steel Research International, 30(11), 2293–2300, 2023. http://doi.org/10.1007/s42243-022-00907-z.

[15] Li, X.; Shonkwiler, S.; McMains, S.: Detection of resin-rich areas for statistical analysis of fiber-reinforced polymer composites. Composites Part B: Engineering, 225, 109252, 2021. http://doi.org/10.1016/j.compositesb.2021.109252.

[16] Long, J.; Shelhamer, E.; Darrell, T.: Fully convolutional networks for semantic segmentation. In Proceedings of the IEEE Conference on Computer Vision and Pattern Recognition, 3431–3440, 2015.

[17] Paredes-Orta, C.A.; Mendiola-Santibañez, J.D.; Manriquez-Guerrero, F.; Terol-Villalobos, I.R.: Method for grain size determination in carbon steels based on the ultimate opening. Measurement, 133, 193–207, 2019. http://doi.org/10.1016/j.measurement.2018.09.068.

[18] Peregrina-Barreto, H.; Terol-Villalobos, I.; Rangel-Magdaleno, J.; Herrera-Navarro, A.; Morales-Hernández, L.; Manríquez-Guerrero, F.: Automatic grain size determination in microstructures using image processing. Measurement, 46(1), 249–258, 2013. http://doi.org/10.1016/j.measurement.2012.06.012.

[19] Rathod, K.; Choudhary, A.K.; Jansche, A.; Ketzer-Raichle, G.; Bernthaler, T.; Schneider, G.: GeGra: Approaching a generic model for quantitative grain size analysis from materials microscopy data using deep learning. Materials Characterization, 217, 114379, 2024. http://doi.org/10.1016/j.matchar.2024.114379.

[20] Ronneberger, O.; Fischer, P.; Brox, T.: U-net: Convolutional networks for biomedical image segmentation. In Medical Image Computing and Computer-Assisted Intervention–MICCAI 2015: 18th international conference, Munich, Germany, October 5-9, 2015, proceedings, part III 18, 234–241. Springer, 2015. http://doi.org/10.1007/978-3-319-24574-4_28.

[21] Sarkar, A.; Prasad, M.; Murty, S.N.: Effect of initial grain size on hot deformation behaviour of Cu-Cr-Zr-Ti alloy. Materials Characterization, 160, 110112, 2020. http://doi.org/10.1016/j.matchar.2019.110112.